Millimeter-level calibration of IMU size effect and its compensation in navigation grade systems

Alexander Kozlov, Fedor Kapralov

Navigation and Control Lab, Lomonosov Moscow State University
Leninskie Gory, 1
119991, Moscow
RUSSIA

Inertial Sensors and Systems 2019
Braunschweig, Germany

978-1-7281-1935-9/19/$31.00 ©2019 IEEE

Abstract

We present a simple method of millimeter-level calibration of inertial measurement unit (IMU) size effect, which proved to be tolerant to most common instrumental errors, including the residual calibration errors of the IMU, and does not require special processing apart from recording standard navigation solution in a special rotations on a turntable. Using the calibration results, we demonstrate the effect of their compensation in an inertial system of navigation grade. Control experiments show that navigation error drops one order of magnitude in certain types of motion as compared to the compensation using IMU design documentation instead of the suggested calibration results.

1. Introduction

Size effect in an inertial measurement unit refers to the spatial separation between points in space where actual specific force components are being measured by single-axis accelerometers. The theory of its effect on navigation solution and its compensation are both well-known and rather straightforward [1–2]. However, the level of accuracy their calibration should obtain is sometimes underestimated. Spatial dimensions taken from the design documentation of the IMU generally have the accuracy level of half a centimeter due to the certain size of accelerometer proof mass itself. It is easily shown that errors of this magnitude in relative proof mass coordinates may produce navigation errors up to several hundred meters in, say, one-hour flight for an intensively maneuvering aircraft. Thus, we suggest considering the compensation problem the other way around. We state it as finding such estimates for accelerometer proof mass coordinates that minimize navigation error when compensating for them.

Since the size effect has a considerable impact on navigation solution only in rotations, especially involving angular accelerations, the IMU should experience same sort of motion in its calibration. There are still several issues exist concerning the calibration procedure. The first one lies in the inability of any rotation table to maintain constant and high angular rate acceleration for a considerable amount of time that desired for the most straightforward approach. The second issue regards to the residual calibration and other instrumental errors of the IMU itself, which tend to contribute to navigation solution in any complex type of motion like the considered above. Although high-end systems available on the market are likely to have this issue completely mitigated, there are few readily available and/or simple descriptions of the appropriate methods and techniques [3].

2. An example of undercompensating the size effect

Suppose there are three accelerometers referred to as “Ax”, “Ay” and “Az”, each having its own point of measurement (sometimes called “the center of percussion”) around their proof masses, as shown in Figure 1. These points of measurement then have their coordinates in the instrumental reference frame, say r_{xx}, r_{xy}, r_{xz} for the “Ax” accelerometer.

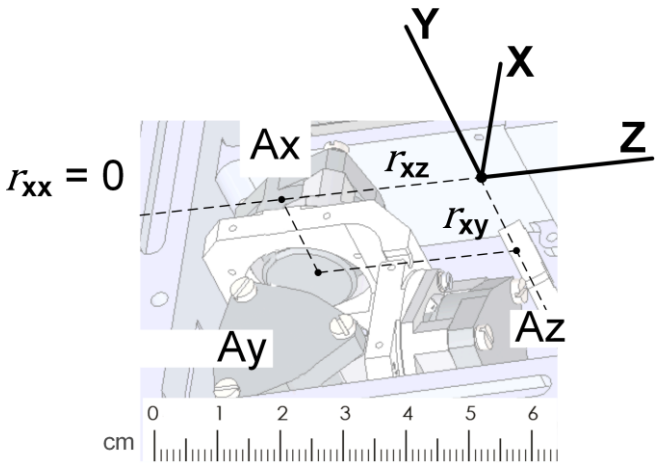

Figure 1. Accelerometer cluster and accelerometer proof mass coordinates.

The equations used to compensate for the accelerometer cluster size effect imply the transition of measured specific force (i.e. proper acceleration) vector components f_x, f_y, f_z to the origin of the instrumental frame (also called the IMU reference center) as follows

$$\begin{aligned} f_x'' &= f_x' - \left[-\left(\omega_y^2 + \omega_z^2\right) r_{xx} + \omega_x \omega_y r_{xy} + \omega_x \omega_z r_{xz} + \dot{\omega}_y r_{xz} - \dot{\omega}_z r_{xy}\right], \\ f_y'' &= f_y' - \left[\ \omega_y \omega_x r_{yx} - \left(\omega_z^2 + \omega_x^2\right) r_{yy} + \omega_y \omega_z r_{yz} + \dot{\omega}_z r_{yx} - \dot{\omega}_x r_{yz}\right], \\ f_z'' &= f_z' - \left[\ \omega_z \omega_x r_{zx} + \omega_z \omega_y r_{zy} - \left(\omega_x^2 + \omega_y^2\right) r_{zz} + \dot{\omega}_x r_{zy} - \dot{\omega}_y r_{zx}\right], \end{aligned} \tag{1}$$

where $f'_{x,y,z}$ denote the specific force components as measured by accelerometers, $f''_{x,y,z}$ represent their corrected (or, to say, compensated) values, and $\omega_{x,y,z}$, $\dot{\omega}_{x,y,z}$ stand for the angular rate components and their time derivatives. Apart from the problem of estimating angular accelerations, the actual values of accelerometer proof masses taken into computation do matter in this procedure. As mentioned above, their typical accuracy ranges up to half a centimeter. Simulating the compensation over a number of real-flight trajectories, it is easy to demonstrate that 5-millimeter deviation in some of the coordinates may generate navigation errors as high as few hundred meters (see Figure 2). Most of solutions in this particular dataset do not experience errors more than 50 meters, which are negligible. But in some cases of highly maneuvering carrier they grow up to 200 meters, and this magnitude may count for high-precision systems.

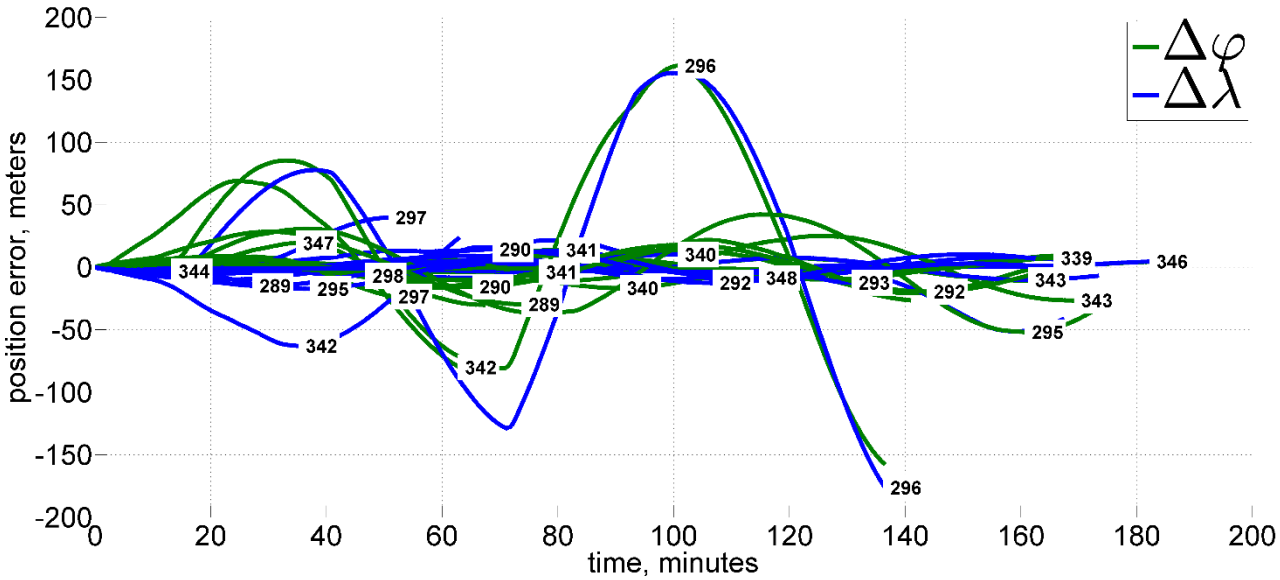

Figure 2. Navigation errors produced by undercompensating some 5 millimeters in one of accelerometer proof mass coordinates, as modeled over 17 flights.

Luckily being systematic, this error becomes the subject to compensation. For that, we need a technique of determining the accelerometer proof mass coordinates with a millimeter-level accuracy. In this context, one cannot directly measure them or take from design documentation due to desired accuracy being considerably smaller than the dimensions of the proof mass itself. Therefore, we should state the problem as getting such estimates for the coordinates in (1) that yield minimum error in navigation solution when compensated for the size effect.

3. Calibration experiment

It is a rather well-known fact, that size effect driven navigation errors emerge mostly in a swaying kind of rotations. To exploit that, we should exert periodic oscillations onto the IMU, so that velocity error growth would have constant rate on average due to the constant (on average) bias in acceleration calculated by navigation algorithm. This growth rate happens to be predictable assuming oscillation parameters known, and linearly relates to the desired coordinates. Thus, their estimates may be obtained almost directly from the velocity plots, without even using a special software for calculations, and with great accuracy provided appropriate conditions. The following sections describe it in more detail.

3.1. Calibration procedures

The IMU works in navigation mode during the experiment. Sitting on a turntable plate, it experiences three cycles of periodic oscillations around the vertical rotation axis. In each cycle, one of instrumental axes points close to the axis of rotation, as Figure 3 suggests.

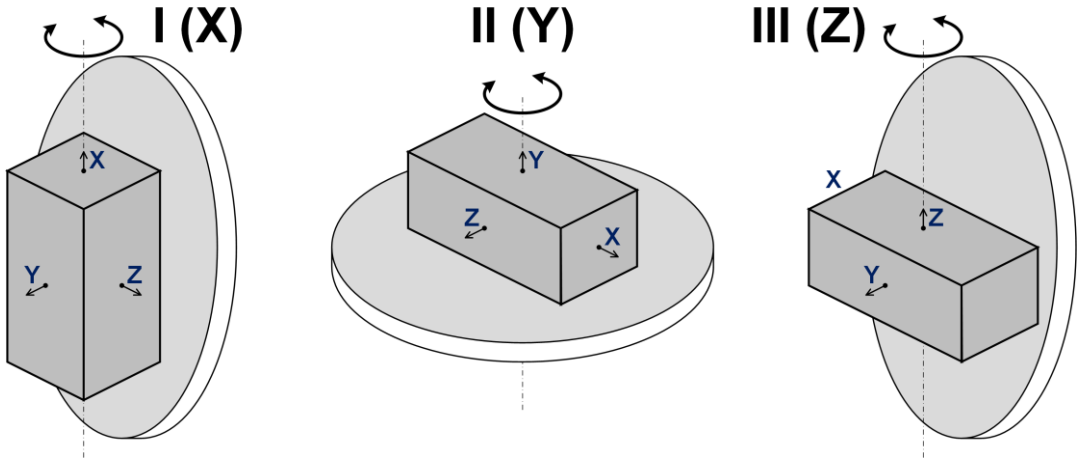

Figure 3. Three cycles of oscillation around vertical axis of rotation in calibration experiment.

Before the oscillation starts, the system performs its regular initial alignment. After that, the navigation output is being recorded at $1–10$ Hz or higher rate whilst swaying begins. As further assessment shows, the oscillation amplitude of $90°$ and periods ranging from 3 to 20 seconds suit well for practical implementation. The oscillation lasts for $5–10$ minutes, which comprise roughly a hundred periods, but still considerably less than a quarter the Schuler period of 84 minutes.

3.2. Notation

To derive the relation between the accelerometer proof mass coordinates being calibrated, and the observable velocity error drift, we introduce the following items listed in Table 1. We take a specific point as IMU reference center. Namely, this is the point of intersection of three planes passing through proof masses of accelerometers orthogonal to their sensitive axes, so that in our notation from above we have $r_{\mathbf{xx}} = r_{\mathbf{yy}} = r_{\mathbf{zz}} = 0$. In fact, virtually any point of the IMU may serve as its reference center, and this particular one is taken just for the sake of symmetry. To transfer from one point to another one should simply alter all coordinates by corresponding constants. The six remaining coordinates stay to be the subject of calibration.

The heading angle is supposed to change as a harmonic function over time. Other types of periodic oscillations also work, but have different relation between accelerometer proof mass spatial separations and observed calculated acceleration. Note that only the time span where the steady oscillations continue does go into further processing. Also, the phase shift of oscillation becomes irrelevant from some point on and therefore excluded from the analysis, since only average values appear in all equations.

Table 1: List of symbols and quantities

Symbol	Name and/or meaning
X, **Y**, **Z**	the first, the second and the third instrumental axis, respectively
E, **N**	East and North directions
Ax, Ay, Az	accelerometers measuring specific force along **X**, **Y** and **Z** directions
$r_{\mathbf{xy}}$, $r_{\mathbf{xz}}$	"Ax" accelerometer proof mass coordinates subject to calibration ($r_{\mathbf{xx}} = 0$)
$r_{\mathbf{yx}}$, $r_{\mathbf{yz}}$	"Ay" accelerometer proof mass coordinates subject to calibration ($r_{\mathbf{yy}} = 0$)
$r_{\mathbf{zx}}$, $r_{\mathbf{zy}}$	"Az" accelerometer proof mass coordinates subject to calibration ($r_{\mathbf{zz}} = 0$)
$V_{\mathbf{E}}$, $V_{\mathbf{N}}$	East and North components of the ground velocity vector calculated by the IMU
$a_{\mathbf{E}}$, $a_{\mathbf{N}}$	East and North components of the calculated ground acceleration vector
t	time
ψ, $\dot{\psi}$, $\ddot{\psi}$	heading angle of the IMU, along with its first and second time derivative
ψ_0, A, T	heading mean value, amplitude and period of oscillations
$\langle \cdots \rangle$	average value of the periodic function inside the angle brackets over its period
$J_1(A)$	Bessel function of the first kind, i.e. $J_1(A) = \langle \sin t \cdot \sin(A \sin t) \rangle$

Under the assumptions stated above, for the IMU heading angle we have:

$$\psi = \psi_0 + A \sin\frac{2\pi t}{T} \quad \Rightarrow \quad \dot{\psi} = A\frac{2\pi}{T}\cos\frac{2\pi t}{T} \quad \Rightarrow \quad \ddot{\psi} = -A\frac{4\pi^2}{T^2}\sin\frac{2\pi t}{T}. \tag{2}$$

3.3. Interpretation

The typical navigation output in the above described experiment looks as Figure 4 shows. In each of the three cycles of oscillations, only two particular accelerometer proof mass coordinates among all six may produce an observable drift in average velocity error. Since linear drift rate is fairly easy to assess, and its coefficient per accelerometer lever arm distance is essentially the same apart from choosing different orientation of the turntable relative to the geodetic grid, one can obtain the desired proof mass coordinates barely from the velocity plots when $\psi_0 = 0, \pm 90°$ or $180°$.

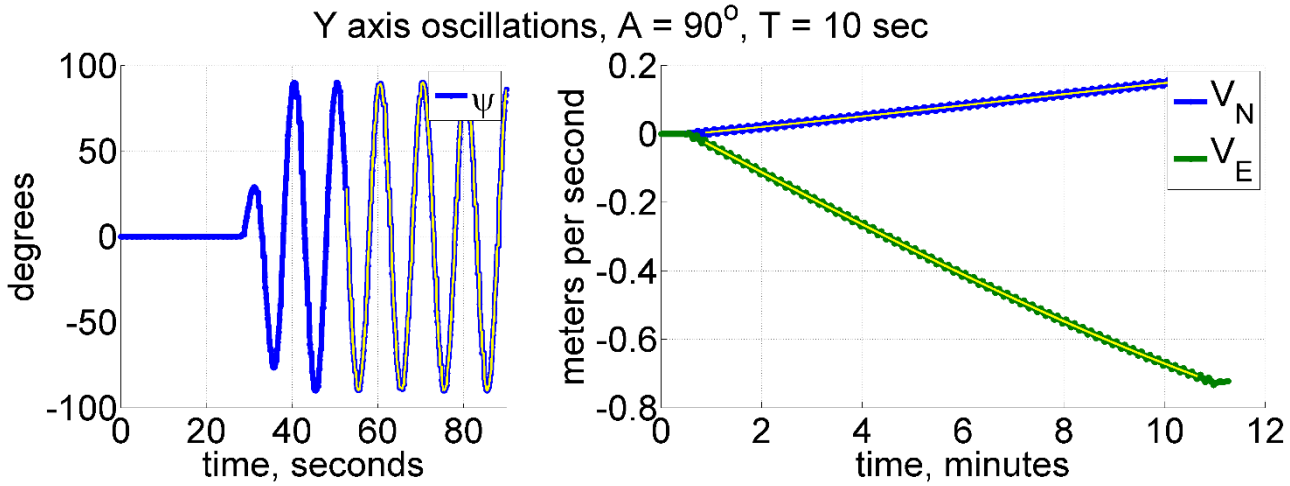

Figure 4. Typical navigation output in the calibration experiment under harmonic oscillations (left). Velocity drift (right) is nearly linear with its rate being proportional to accelerometer proof mass spatial separation. Yellow line marks the time span used for size effect calibration.

We will now express corresponding relations for each cycle of oscillations around the vertical axis of rotation. Axis directions, accelerometer locations and their coordinates in those cycles are shown in Figure 5 below. We use the conventional right-handed airborne reference frame, where the first axis, **X**, is longitudinal pointing forward, the second one, **Y**, heads upwards perpendicularly to the wing plane, and the third one, **Z**, is lateral.

For the case of **X** axis being the axis of rotation, to avoid the gimbal lock, i.e. the ambiguity of IMU roll and heading angles when **X** axis lines up vertically, we assume keeping the pitch angle slightly lower than $90°$ but positive, as featured in the left diagram of Figure 5.

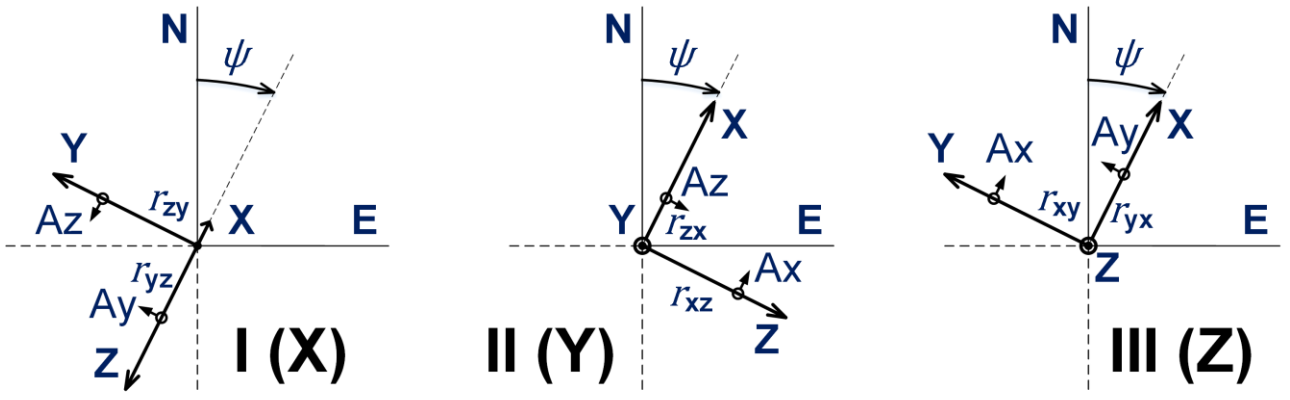

Figure 5. Axis directions, accelerometer locations and their coordinates in each calibration cycle.

In our notation, the calculated acceleration due to accelerometer cluster size effect will have its components as given in (3)–(5). Substituting then the dynamics of oscillations from (2) into them, and also averaging over the oscillation period, yield (7)–(9).

For **X** axis oscillations:

$$\begin{array}{rcl} a_{\mathbf{y}} &=& r_{\mathbf{yz}}\ddot{\psi}, \\ a_{\mathbf{z}} &=& -r_{\mathbf{zy}}\ddot{\psi}, \end{array} \Rightarrow \begin{array}{rcl} a_{\mathbf{E}} &=& -a_{\mathbf{y}}\cos\psi - a_{\mathbf{z}}\sin\psi, \\ a_{\mathbf{N}} &=& a_{\mathbf{y}}\sin\psi - a_{\mathbf{z}}\cos\psi. \end{array} \tag{3}$$

For **Y** axis oscillations:

$$\begin{array}{rcl} a_{\mathbf{z}} &=& r_{\mathbf{zx}}\ddot{\psi}, \\ a_{\mathbf{x}} &=& -r_{\mathbf{xz}}\ddot{\psi}, \end{array} \Rightarrow \begin{array}{rcl} a_{\mathbf{E}} &=& a_{\mathbf{z}}\cos\psi + a_{\mathbf{x}}\sin\psi, \\ a_{\mathbf{N}} &=& -a_{\mathbf{z}}\sin\psi + a_{\mathbf{x}}\cos\psi. \end{array} \tag{4}$$

For **Z** axis oscillations:

$$\begin{array}{rcl} a_{\mathbf{x}} &=& r_{\mathbf{xy}}\ddot{\psi}, \\ a_{\mathbf{y}} &=& -r_{\mathbf{yx}}\ddot{\psi}, \end{array} \Rightarrow \begin{array}{rcl} a_{\mathbf{E}} &=& a_{\mathbf{x}}\sin\psi - a_{\mathbf{y}}\cos\psi, \\ a_{\mathbf{N}} &=& a_{\mathbf{x}}\cos\psi + a_{\mathbf{y}}\sin\psi. \end{array} \tag{5}$$

We define then:

$$c(A,T) = {}^{T^2}\!/_{4\pi^2 A \cdot J_1(A)} \tag{6}$$

to be the coefficient corresponding to the particular oscillation pattern. Therefore, (3)–(6) imply the following expressions for the coordinates subject to calibration, given in matrix form.

For **X** axis oscillations:

$$\begin{bmatrix} r_{\mathbf{zy}} \\ r_{\mathbf{yz}} \end{bmatrix} \approx c(A,T) \cdot \begin{bmatrix} -\cos\psi_0 & \sin\psi_0 \\ -\sin\psi_0 & \cos\psi_0 \end{bmatrix} \cdot \begin{bmatrix} \langle a_{\mathbf{E}} \rangle \\ \langle a_{\mathbf{N}} \rangle \end{bmatrix}. \tag{7}$$

For **Y** axis oscillations:

$$\begin{bmatrix} r_{\mathbf{xz}} \\ r_{\mathbf{zx}} \end{bmatrix} \approx c(A,T) \cdot \begin{bmatrix} \cos\psi_0 & -\sin\psi_0 \\ \sin\psi_0 & \cos\psi_0 \end{bmatrix} \cdot \begin{bmatrix} \langle a_{\mathbf{E}} \rangle \\ \langle a_{\mathbf{N}} \rangle \end{bmatrix}. \tag{8}$$

For **Z** axis oscillations:

$$\begin{bmatrix} r_{\mathbf{yx}} \\ r_{\mathbf{xy}} \end{bmatrix} \approx c(A,T) \cdot \begin{bmatrix} \sin\psi_0 & \cos\psi_0 \\ -\cos\psi_0 & \sin\psi_0 \end{bmatrix} \cdot \begin{bmatrix} \langle a_{\mathbf{E}} \rangle \\ \langle a_{\mathbf{N}} \rangle \end{bmatrix}. \tag{9}$$

That means having the estimates for mean accelerations $\tilde{a}_{\mathbf{E}}$, $\tilde{a}_{\mathbf{N}}$ from the velocity plots like those in Figure 4 for all three calibration cycles, one immediately obtains estimates $\tilde{r}_{\mathbf{zy}}$, $\tilde{r}_{\mathbf{yz}}$, $\tilde{r}_{\mathbf{xz}}$, $\tilde{r}_{\mathbf{zx}}$, $\tilde{r}_{\mathbf{yx}}$, $\tilde{r}_{\mathbf{xy}}$ for accelerometer proof mass coordinates to be used in compensation (1).

The error budget directly follows from (7)–(9) and appears to considerably depend on the oscillation parameters. Namely, it is $\Delta r = c(A,T) \cdot \Delta a$. Hence, for, say, 90 degree amplitude and the period of 5 seconds, $c(A,T)$ amounts to around 0.7. Therefore, every 0.1 millimeter

per second squared error in estimating the acceleration (which is roughly 0.1 meters per second error in measuring velocity over a 10 minute interval) yields about 0.1 millimeter error in coordinates.

4. Mitigating the instrumental error contribution

According to the above approximation, some sub-millimeter accuracy seems to be easily achievable, still limited in the real world application though. And the primary reason for the limitation arises from the systematic errors of inertial sensors and other instrumentation, which also tend to contribute to the velocity error. And rather complex motion involved in the experiment exaggerates this effect even more. However, we discovered both by analytical approximations and by numerical tests that the contribution of systematic sensor error terms to the velocity error appears to stay the same on average when the period of oscillation changes. And this fact allows making the calibration insensible at least to the conventional systematic instrumental errors. More details follow in the next section.

4.1. Instrumental error contribution

In inertial navigation technology, the magnitude of calculated velocity error within 0.1–0.2 meters per second under intense maneuvering is generally considered as acceptable on a time scales of substantial fraction of an hour or more. As shown before, depending on the parameters of oscillations such error may bias the results in the considered calibration experiment. Figure 6 represents an example of the numerically simulated velocity error gain due to non-orthogonal gyroscope sensitive axes along the instrumental **X** and **Y** directions. Remarkably, this error stays effectively the same when the period of oscillation changes (see the right pane in Figure 6).

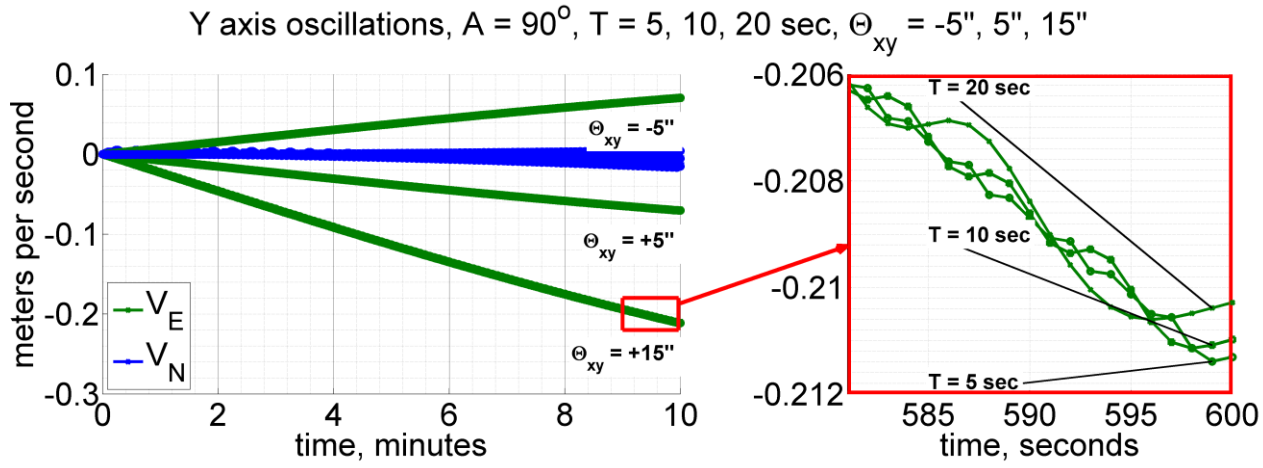

Figure 6. Velocity error growth in the calibration experiment under a simulated axial misalignment Θ_{xy} of **Y** gyroscope towards **X** axis by 5″–15″. Right pane zooms in the red rectangle on the left.

In this study, we have considered the following conventional error sources [4]:

- gyroscope constant drifts;
- accelerometer null bias;
- accelerometer and gyroscope scaling factor errors;
- axial misalignments of their sensitive axes;
- axial misalignment between the IMU and the rotation table plate;
- axial misalignment between axes of the rotation table and their intended directions.

All instrumental errors listed above are assumed to be small enough for the linear navigation error equations to hold [5]. As above stated, the impact of all kinds of error sources from the above list on navigation solution in the calibration experiment appears to be either negligible or independent to the period of oscillations. The complete rationale of this fact lies out of the scope of this manuscript due to its limited volume. To put it short, we have verified it in two ways. Firstly, by analytical approximation, i.e. by taking linear error equations and applying the technique of averaging them over the oscillation period for the particular kind of IMU motion. The second method involved extensive numerical simulations like that shown in Figure 6, which totally confirmed analytical derivation and the assumptions taken.

4.2. Cancelling the instrumental error terms

At this point, knowing that at least for the conventional systematic instrumental errors their contribution to navigation solution deviation stays the same on average under the period of oscillations being changed, we may suggest how to cancel them. One needs just to carry out calibration experiments with two different periods (with other parameters unchanged), and then difference their results. Let T_1 and T_2 be the periods of oscillations, e.g. $T_1 = 5$ and $T_2 = 10$ seconds. Then, the final instrumental error-free relation comes as follows:

$$\begin{bmatrix}\tilde{r}_{..}\\ \tilde{r}_{..}\end{bmatrix} = \big(c(A,T_1) - c(A,T_2)\big) \cdot R(\psi_0) \cdot \begin{bmatrix}\tilde{a}_{\mathrm{E}}(T_1) - \tilde{a}_{\mathrm{E}}(T_2)\\ \tilde{a}_{\mathrm{N}}(T_1) - \tilde{a}_{\mathrm{N}}(T_2)\end{bmatrix}, \tag{10}$$

where $\tilde{r}_{..}$ symbols stand for the estimates of whatever coordinates from (7)–(9), and R is an appropriate rotation matrix from the same equation.

5. Results

We applied the calibration procedure described in previous sections to a ring laser gyro-based inertial unit of $\sim 1-2$ nm/hr grade. It has already the compensation of size effect implemented according to (1), but with the accelerometer proof mass coordinates taken from its design documentation. Corrections obtained by the calibration method according to (10) appeared to extend from 2.4 to 6.9 millimeters for different coordinates.

After that, a new version of IMU firmware was prepared with accelerometer proof mass coordinates in (1) amended. Then both versions, the old and the new one, went through the same kind of control experiments. They included five intensive back-and-forth $180°$ turns made manually by hand in three different positions. Those turns were neither symmetric, nor periodic, but were sort of similar every time. Due to intensive manner of rotations involved, the navigation solution experienced a considerable accumulation of velocity error. Figure 7 summarizes the comparison of those error's magnitude for two firmware versions. All in all, using the newly calibrated size effect compensation reduced the error gain roughly by an order of magnitude under this particular motion pattern. In the real world, the carrier does not experience such a rapid attitude variations, so the effect would be smaller, or even inconsiderable in some cases (see Figure 2). However, we believe that being completely systematic, it deserves to be compensated at all times.

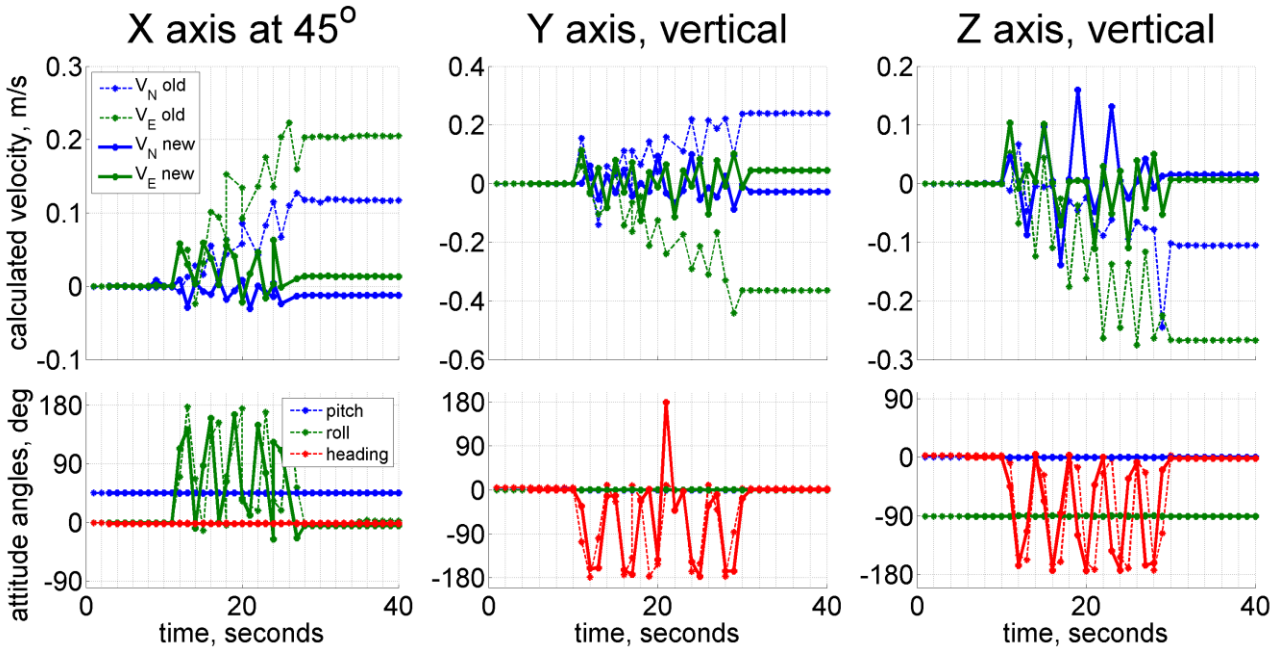

Figure 7. Velocity error gain using old and new size effect compensation in three test experiments, each of five intensive back and forth $180°$ turns around one instrumental axis. Errors appear to be reduced by a factor of roughly 10. Rotation axis positions are specified at top. 1 Hz sampling rate.

6. Conclusion

We described a simple procedure for the millimeter-level accelerometer cluster size effect calibration for an inertial measurement unit of navigation grade. In this procedure, all conventional instrumental errors do not affect the final estimate. The results suggest that in certain types on maneuvering the navigation error drops as low as one order of magnitude smaller compared to the size effect compensation based on the design documentation of the IMU. For a real flight trajectories we expect this to eliminate some few hundred meters of systematic position error.

References

[1] Hung J.C., Hunter J.S., Stripling W.W., White H.V., “Size effect on navigation using a strapdown IMU”, Technical report T-79-73. Redstone Arsenal, Alabama, USA: U.S. Army missile research and development command, 1979.

[2] Eilon S., “A least squares approach to size effect in inertial navigation” // Position, Location and Navigation Symposium — PLANS 2014. Monterey, California, USA: IEEE/ION, 2014. P. 721–732.
DOI: 10.1109/PLANS.2014.6851438.

[3] Gao P., Li K., Wang L., Liu Z., “A self-calibration method for tri-axis rotational inertial navigation system” // IEEE Transactions on Industrial Electronics. 2018. Vol. 65, Issue 2. P. 1655–1664.
DOI: 10.1109/TIE.2017.2733491.

[4] Kozlov A., Sazonov I., Vavilova N., “IMU calibration on a low grade turntable: Embedded estimation of the instrument displacement from the axis of rotation” // 2014 International Symposium on Inertial Sensors and Systems (ISISS), Laguna Beach, California, USA: IEEE, 2014. P. 1–4.
DOI: 10.1109/ISISS.2014.6782525.

[5] Golovan A.A., Demidov O.V., Vavilova N.B, “On GPS/GLONASS/INS tight integration for gimbal and strapdown systems of different accuracy” // IFAC Proceedings Volumes. 2010. Vol. 43, Issue 15. P. 505–509.
DOI: 10.3182/20100906-5-JP-2022.00086.